HEFAT2012
9th International Conference on Heat Transfer, Fluid Mechanics and Thermodynamics
16 – 18 July 2012
Malta

HIGH-FIDELITY MODELING OF SYNTHETIC JET ACTUATORS FOR AIRFOIL FLOW AND NOISE CONTROL

Golubev V.V* and Mankbadi R.R.
*Author for correspondence
Department of Aeronautical Engineering,
Embry-Riddle Aeronautical University,
Daytona Beach, FL 32114
USA,
E-mail: golubd1b@erau.edu

ABSTRACT

Synthetic jet actuators (SJAs) may be carefully designed to alleviate the negative impact of impinging flow non-uniformities on the aircraft wing performance. The current work investigates the effectiveness of SJAs for control of a low-speed airfoil unsteady aerodynamic response and acoustic radiation both for the clean upstream flow conditions and in the presence of an upstream flow disturbance. In the high-fidelity numerical studies of flow and noise control of, respectively, SD7003 and Joukowski airfoils in laminar and transitional flow regimes, the actuator is modeled without its resonator cavity by imposing a simple fluctuating-velocity boundary condition at the bottom of the actuator's orifice. The orifice with the properly defined boundary condition is then embedded into the airfoil surface for conducting high-accuracy viscous analysis of SJA-based active flow and noise control. Results of low Reynolds number numerical simulations indicate that the SJA effect on unsteady airfoil response appears most significant for the actuator operating in resonance with the airfoil natural shedding frequency.

INTRODUCTION

An airfoil unsteady aerodynamic response coupled with its acoustic radiation is highly dependent on the flow regime. In the absence of upstream flow non-uniformities, the dominant mechanism of trailing-edge noise radiation at high Reynolds numbers is commonly related to the acoustic scattering of the airfoil turbulent boundary layer convecting at the airfoil's trailing edge. The acoustic radiation process then involves transforming the quadrupolar (acoustically inefficient) nature of convected eddies into much more acoustically efficient dipolar sources [1] still producing generally moderate noise levels. The same mechanism, however, can give rise to distinct, highly pronounced tones when the airfoil boundary layer remains in a transitional state and may result in flow-acoustic resonance phenomena associated with interaction between upstream-propagating acoustic waves scattered at the trailing edge and the growing boundary-layer instability waves [2-3].

On the other hand, when a realistic airfoil encounters a region of highly-nonuniform unsteady flow, its noise radiation pattern exhibits the interference of both leading-edge and trailing-edge acoustic sources [4], and the impact of the incoming unsteady flow disturbances may also interfere and even trigger the viscosity-dominated trailing edge noise sources either through enhanced boundary layer dynamics and/or the impact from the leading-edge acoustic scattering. Furthermore, for the airfoil abruptly entering into stall (e.g., due to encounter with a sudden wind draft generally modeled by a sharp-edge gust), its acoustic signature drastically changes due to the presence of a massively separated flow. The complexity and variety of airfoil acoustic phenomena is evident and has been addressed in a number of previous works.

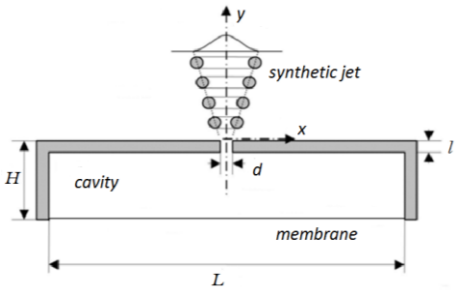

Figure 1. Schematic of synthetic-jet actuator.

To this day, the primary methods of airfoil noise control have involved mostly passive means such as leading and trailing edge serrations. The current work numerically investigates effectiveness of synthetic-jet actuators (Fig. 1) embedded in the airfoil surface for active control of airfoil coupled unsteady aerodynamic and aeroacoustic response.

In the first part of the study, the effect of SJA actuation on unsteady aerodynamic response in presence of a high-amplitude upstream flow disturbance is investigated for laminar SD7003 airfoil. In the second part of the work, the developed approach to model SJA actuator is employed for active noise control of transitional Joukowski airfoil in uniform and non-uniform flow.

NUMERICAL MODEL

The effects of synthetic-jet actuation applied to low-Re unsteady flow over airfoil is analyzed using a high-accuracy three-dimensional, compressible viscous solver [5] used in our previous gust-airfoil and vortex-airfoil interaction studies [6-8]. The following features of the employed numerical procedure appear particularly beneficial for the current application:

- Implicit time marching algorithms (up to 4^{th}-oder accurate) are suitable for the low-Re wall-bounded flows.
- High-order spatial accuracy (up to 6^{th}-order accurate) is achieved by use of implicit compact finite-difference schemes, thus making LES resolution attainable with minimum computational expense.
- Robustness is achieved through a low-pass Pade-type non-dispersive spatial filter that regularizes the solution in flow regions where the computational mesh is not sufficient to fully resolve the smallest scales. Note that the governing equations are represented in the original unfiltered form, used unchanged in laminar, transitional, or fully turbulent regions of the flow. The resulting Implicit LES (ILES) procedure employs the high-order filter operator in lieu of the standard SGS and heat flux terms. The resulting filter thus selectively damps the evolving poorly resolved high-frequency content of the solution.
- Overset grid technique is adopted for geometrically complex configurations, with the high-order interpolation maintaining spatial accuracy at overlapping mesh interfaces.

The approach was previously tested against various benchmarks [5] and was successfully employed in flow control predictions, e.g., by Rizzetta et al [9]. The current version of the code employs the developed and successfully tested capability for the high-fidelity analysis of unsteady flow-structure interactions including accurate descriptions of upstream unsteady vortical flowfields used in the current study.

NUMERICAL IMPLEMENTATION

Two high-fidelity numerical studies were conducted to investigate SJA-based airfoil active flow and noise control. In the code numerical implementation, all variables are non-dimensionalized by the airfoil chord *c*, freestream flow density ρ_∞ and flow velocity u_∞. All results are obtained from the code parallel simulations using ERAU's Beowulf Zeus cluster (64-bit, 3.2 GHz Intel Xeon, 4GB RAM systems), with the mesh efficiently partitioned into 96 overlapped blocks assigned to different processors.

Flow Control of SD7003 Airfoil

Two-dimensional numerical simulations with embedded actuator model are performed for unsteady flow around stationary SD7003 airfoil in the laminar flow regime with Mach and Reynolds numbers M=0.1 and Re=10,000, respectively. A fixed dimensionless time step with $\Delta t = 2\times10^{-4}$ is chosen for the implicit time marching. Based on the analyses of Refs [6-8], 466 × 395 × 3 grid is employed with a refined clustering on the suction side especially towards the trailing edge for more accurate resolution of the enhanced boundary-layer vorticity dynamics and its shedding into the wake (Fig. 2, top plot).

In computations, the freestream conditions are imposed at the farfield boundary located more than 100 chords away from the airfoil, with the grid rapidly stretching towards that boundary to ensure effective elimination of spurious reflections achieved in conjunction with the low-pass spatial filtering [5].

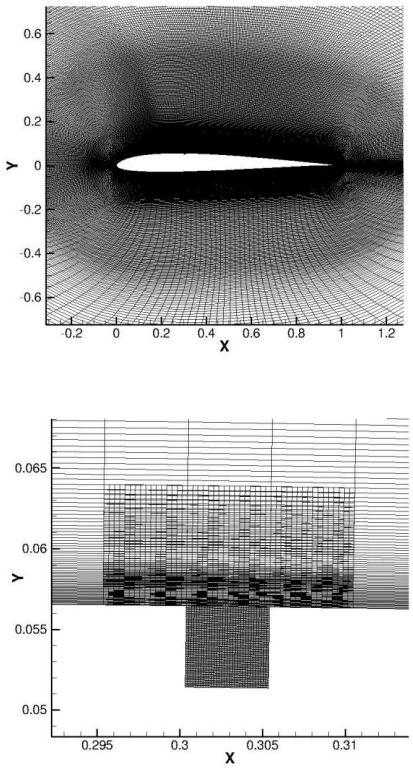

Figure 2. Top: SD7003 airfoil sectional 466 × 395 grid; bottom: Details of overset meshes in SJA orifice region.

Modeling of the synthetic-jet actuator is realized through embedding the actuator's orifice mesh in the airfoil surface and providing an adequate overlap with the original airfoil mesh as shown in Fig. 2 (bottom plot). The proper implementation of the employed overset grid methodology involves 6 meshes generated using Pointwise© software in the near-orifice overlap region. The overset grid connectivity is established using NASA's PEGASUS [10] and AFRL's BELLERO [11] software, with the connectivity data produced by the former serving as input for the latter handling grid decomposition and establishing the intra-grid communication required for the grid

system subdivided into blocks for parallel processing. More details of the employed overset mesh procedures can be found in Ref. [11].

In this study, the embedded actuator model is located about 0.3*c* downstream from the leading edge on the airfoil suction side in the area where a laminar separation zone forms based on the steady-state simulations, as observed in Fig. 3. The ratio of the orifice width to the airfoil chord in this study is fixed at *d*/*c*=0.005.

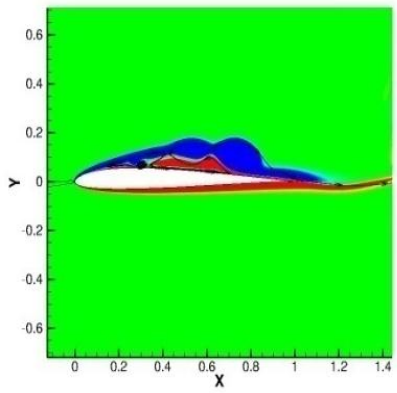

Figure 3. Vorticity contours and streamlines for SD7003 airfoil steady-state flow condition without actuation.

With the SJA orifice mesh embedded in the airfoil surface, the adopted numerical procedure imposes boundary conditions at the bottom of the orifice. Note that such approach accounts for the effect of grazing flow that modifies the jet structure at the actuator's orifice exit, which thus precludes specifying the fluctuating jet velocity at the orifice exit. To further simplify the numerical formulation, the current test study follows Ref. [12] which suggests imposing a simple time-harmonic velocity fluctuation thus achieving a good comparison with results obtained from the full actuator cavity simulations. A single velocity component normal to the orifice bottom is considered in the current work. In test simulations, a value of 15m/s is assumed for the latter. Hence, with the solver non-dimensionalization, the following simple expression for the resulting fluctuating velocity at the bottom of the orifice is employed (ω_a is the actuation frequency),

$$v_{SJA} = 0.5\cos(\omega_a t) \qquad (1)$$

In numerical simulations, the actuation of the flow starts at *t*=15, simultaneously with generation of a gust in cases with the imposed upstream flow disturbance.

Noise Control of Joukowski Airfoil

For analysis of airfoil noise radiation and its active control, this study employs a Computational Aeroacoustics (CAA) benchmark problem of inviscid time-harmonic gust interaction with symmetric Joukowski airfoil [13]. A 649 × 395 × 3 mesh generated around the airfoil is employed and shown in Fig. 4 (top) for the near-surface region. The overall grid topology and boundary conditions are similar to the previous case of SD7003 airfoil. Such a fine near-field mesh in the current case study is required to provide an accurate resolution of the boundary-layer vorticity dynamics and acoustic waves which at certain flow conditions may interact to form a self-sustained feedback loop. In fact, such resonance mechanism that was experimentally and numerically explored in Ref. [4] for NACA 0012 airfoil has also been suspected to dominate in the trailing-edge noise radiation observed in the transitional flow regime over Joukowski airfoil in Refs [4, 14].

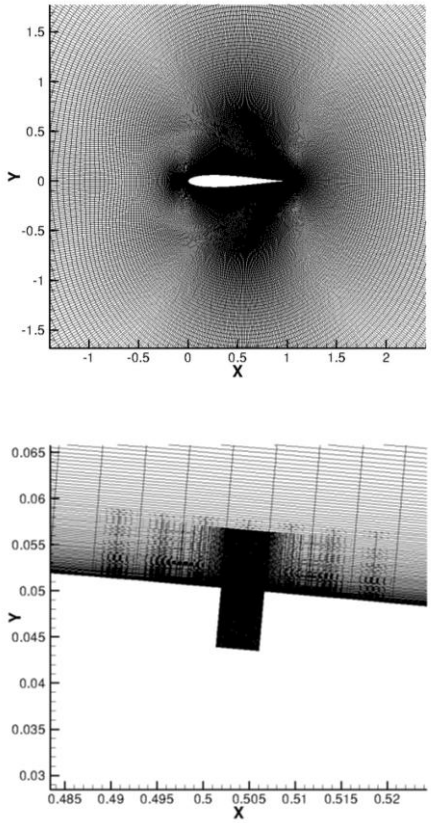

Figure 4. Top: Joukowski airfoil sectional 649 × 395 grid; bottom: Details of overset meshes in SJA orifice region.

The outlined above SJA modelling procedure is also incorporated in the noise control study, with the actuator model in Fig. 4 (bottom) embedded at the mid-chord location and excited according to Eq. (1). In numerical simulations, the actuation of the flow starts at *t*=40, simultaneously with generation of a gust in cases with imposed upstream flow disturbance.

Sharp-Edge and Time-Harmonic Gust Models

To model the effect of the unsteady upstream flow, two gust models are investigated in this study corresponding to the sharp-edge gust and time-harmonic gust (Fig. 5). The former may represent a sudden wind draft with prescribed duration which for high gust amplitudes may inflict a stalled airfoil flow condition [7]. The latter represents a fluctuating vortical disturbance induced, e.g., by the wake from an upstream body.

Both types of gust are generated upstream of the airfoil using an efficient momentum source method described in Ref. [6].

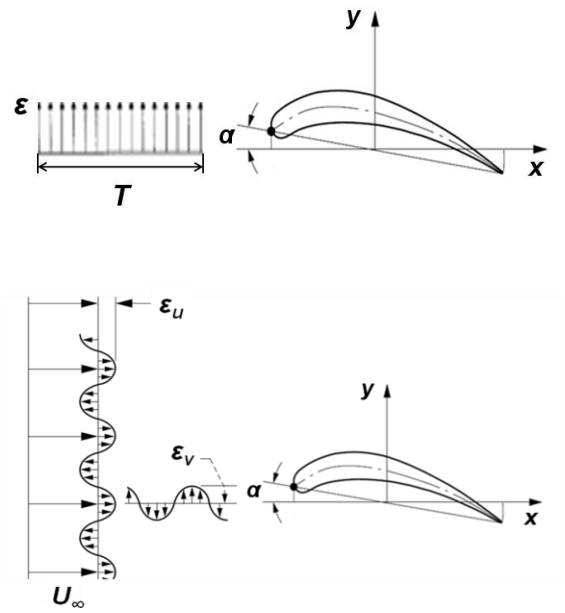

Figure 5. Sharp-edge (top) and time-harmonic (bottom) gust-airfoil interaction models.

The generated gust perturbation fields are described in terms of the following velocity components,

$$v_g(x,t) = \begin{cases} \varepsilon_g, & u_\infty (t - T_g) \le x \le u_\infty t \\ 0, & otherwise \end{cases} \qquad (2)$$

for the sharp-edge gust's upwash component, and

$$u_g(x,y,t) = \varepsilon_u \cos(\alpha x + \beta y - \omega_g t)$$
$$v_g(x,y,t) = \varepsilon_v \cos(\alpha x + \beta y - \omega_g t) \qquad (3)$$

where

$$\varepsilon_u = -\left(\frac{\varepsilon_g \beta U_\infty}{\sqrt{\alpha^2 + \beta^2}} \right), \qquad \varepsilon_v = \left(\frac{\varepsilon_g \alpha U_\infty}{\sqrt{\alpha^2 + \beta^2}} \right),$$

for the time-harmonic gust's streamwise and upwash components, respectively. In (2) and (3), ε_g and T_g are, respectively, the gust amplitude and duration. For the time-harmonic gust, additional parameters include α and β, the gust wave numbers in the x and y directions, and ω_g, the gust frequency. Note that $\alpha = \omega_g / U_\infty$ and $\beta = \alpha \tan \chi$, where χ is the angle between the normal vector of the gust phase front and the x-axis.

SD7003 AIRFOIL FLOW CONTROL SIMULATIONS

The first part of the study investigates effect of SJA actuation on SD7003 airfoil unsteady response in a non-uniform flow with M=0.1 and Re=10,000. The background steady-state flow corresponds to the airfoil installed at the angle of attack $\alpha=8^0$ thus nearing the stall condition. The steady-state flowfield is first obtained by marching in time for 15-20 characteristic cycles (based on the wake-shedding Strouhal number, $St_\alpha=f_s\, c \sin\alpha / u_\infty \sim 0.2$) to guarantee a time-asymptotic nearly-periodic state.

The time-periodic unsteady forcing of the airfoil boundary layer with the velocity profile (1) imposed at the bottom of the embedded actuator's orifice results in a modification of the vorticity dynamics and the corresponding aerodynamic responses. Fig. 6 (left) illustrates the vorticity contours near the SJA orifice area revealing the fluctuating jet velocity during the jet expulsion phase obtained for actuation frequency ω_a=12.6 with unperturbed upstream flow. Note how the jet interaction with the grazing flow completely modifies the axisymmetric jet structure in comparison with the case of SJA performance in a quiescent medium. The time history of the unsteady aerodynamic lift in Fig. 6 (right) also indicates a noticeable effect of actuation.

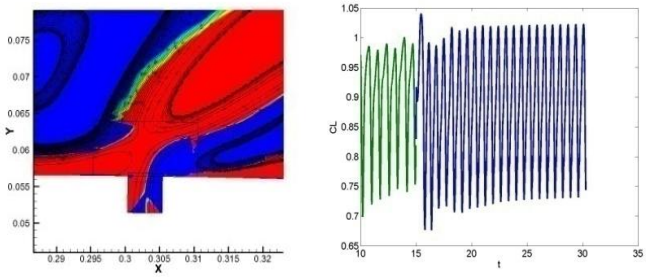

Figure 6. Instantaneous vorticity contours with streamlines (left) and the unsteady lift time history (right) over the actuation period corresponding to ω_a=9.

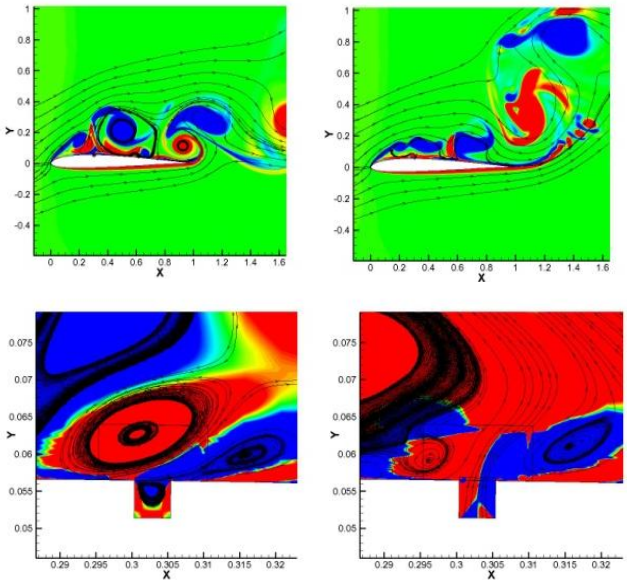

Figure 7. Vorticity contours and streamlines over the actuation period with SJA off (left plots) and on (right plots) for gust-stalled airfoil, ω_a=12.6.

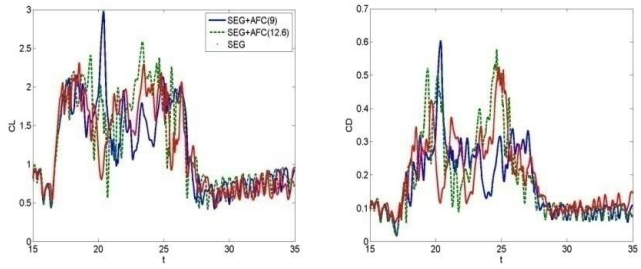

Figure 8. Airfoil unsteady lift (left) and drag (right) responses to SEG with SJA off and on (ω_a=9 and 12.6).

With the incident sharp-edge gust imposed with amplitude ε_g =0.35 and duration T_g=5 in Eq. (2), impinging on the airfoil surface, the pattern of the boundary-layer vorticity dynamics dramatically changes as illustrated in Fig. 7 with SJA off (left plots) and on with ω_a=12.6 (right plots). The stalled airfoil unsteady response appears sensitive to the actuation frequency as observed in Fig. 8 comparing the unsteady lift and drag responses at ω_a=9 and ω_a=12.6 against the gust response without actuation. Note that the peak response values with SJA on appear primarily shifted and in some cases even increased, hence indicating a limited SJA control authority with such actuation regime when applied to a massively separated flow. However, it is important to note that the airfoil's recovery back to the steady-state oscillations following the gust passage appears to be expedited by actuation.

It is important to note that for SJA actuation with ω_a=9 close to the shedding frequency, the results in Fig. 8 show a sudden dominant peak followed by a significantly subdued response afterwards. This may reveal benefits of the actuation regime resonant with oscillating steady-state flow condition.

JOUKOWSKI AIRFOIL NOISE CONTROL SIMULATIONS

In the second part of the study, the predicted unsteady aerodynamic and aeroacoustic responses are compared against the corresponding validated CAA benchmark problem solutions obtained for inviscid time-harmonic gust interaction with symmetric, 12%-thick, unloaded Joukowski airfoil at Mach number M=0.5 [15]. The results are examined and compared for the 2D gust (3) with amplitude ε_g =0.1 convecting with the mean flow with the gust phase angle χ=45^0 and oscillating with reduced frequency $k_g=\omega_g c/2u_\infty$=1. With the code's non-dimensionalization, the corresponding gust parameters are $\alpha = \beta = \omega_g = 2k_g = 2$.

The study considers a transitional flow case with Re=50,000 previously addressed in Ref. [14]. With the uniform upstream flow conditions, the airfoil unsteady response during such flow regime exhibits a very high boundary-layer receptivity to flow perturbations. To illustrate some general response features, Fig. 9 first compares the lift time histories without impinging gust showing that the embedded actuator cavity by itself (without actuation) dramatically changes the mean and the amplitude of the unsteady lift response. Both cases exhibit a complicated periodic pattern associated with the unstable laminar separation region formed at the trailing edge and periodically switching its primary position between the airfoil suction and pressure sides (Fig. 10). Such separation zones are associated with amplified boundary-layer instabilities developing into large vortical structures. As noted in Ref. [12], such structures are continuously generated and convected past the trailing edge inducing high-amplitude wake vorticity oscillations and scattering at the trailing edge into acoustic waves. It thus appears that the mere presence of the actuator cavity on the suction side not only creates a significant positive lift bias at this flow regime but may also modify both the RMS surface pressure distribution and the airfoil acoustic radiation.

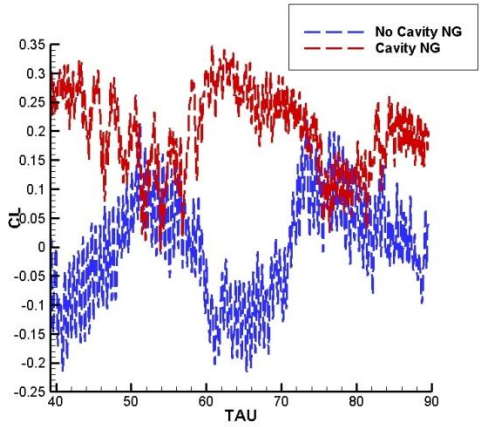

Figure 9. Airfoil lift response with (red line) and without (blue line) embedded SJA cavity (no gust, no actuation).

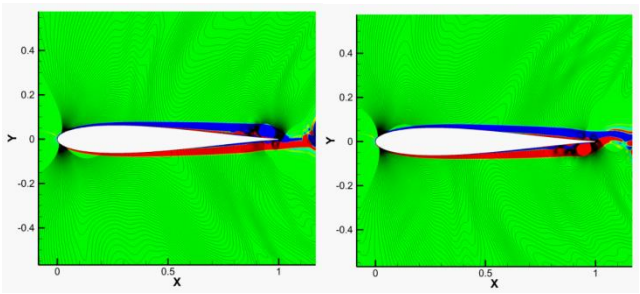

Figure 10. Vorticity/pressure contours showing separation regions at different moments of time (no gust, no cavity).

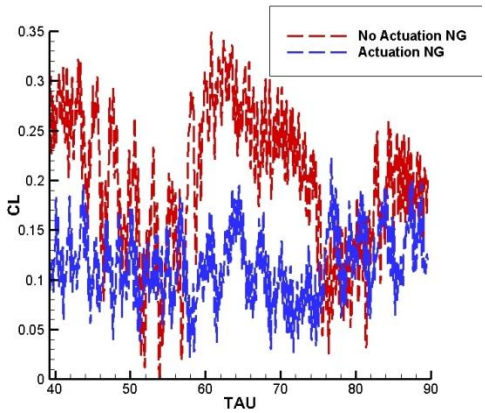

Figure 11. Airfoil lift response with (blue line) and without (red line) actuation, with embedded SJA cavity (no gust).

A time-periodic SJA actuation (implemented in this work in resonance with the shedding frequency ω_a = 10.47 in Eq. (1)) produces a regularizing effect on the airfoil lift response (Fig. 11) associated with continuously energized boundary layer on the suction side. Fig. 12 shows streamlines and vorticity contours illustrating the instantaneous actuation effect on the boundary layer dynamics.

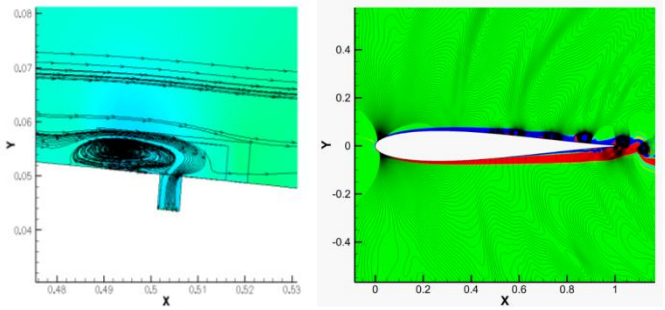

Figure 12. Effect of actuation on boundary-layer vorticity.

With impinging gust, the airfoil response appears to be completely dominated by the time-periodic forcing with gust frequency with superimposed fluctuations at the wake shedding frequency. The analysis indicates that the gust, in fact, induces a phase-locking mechanism triggering a time-periodic generation and shedding of large vortical structures on both sides of the airfoil in synch with the gust frequency.

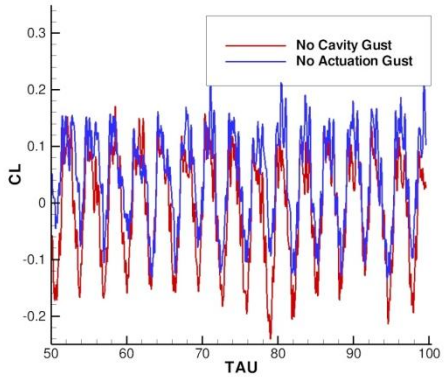

Figure 13. Airfoil lift response to incident gust with (blue line) and without (red line) embedded SJA cavity (no actuation).

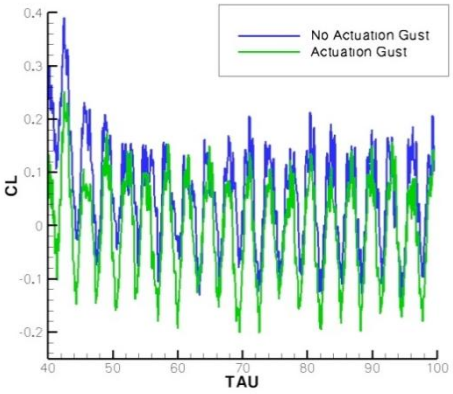

Figure 14. Airfoil lift response to incident gust with (green line) and without (blue line) SJA actuation.

As a result of the gust-dominated wake shedding pattern, the presence of the cavity and its actuation appear less significant with the current selection of SJA location, as observed in Figs. 13-14. However, their effects on the fluctuating lift amplitudes are still noticeable.

SJA Effect on Airfoil Aerodynamics and Noise

For a more detailed analysis of the actuation effects on the transitional airfoil aerodynamic and acoustic responses, the results presented below compare the current 2D numerical viscous solutions obtained with uniform upstream flow conditions (dashed lines) and with the impinging gust (solid lines) against validated inviscid CAA benchmark gust response solutions (black lines) from Ref. [15]. The cases with embedded non-actuated cavity are compared against the corresponding cases with SJA actuation. All results are obtained based on FFT analysis of data samples collected (once all the transients are removed) for the period T=50 with the FFT frequency resolution of $\Delta\omega \approx 0.126$.

The time-averaged mean pressure distributions on the airfoil surface in Fig. 15 (top) show close similarity with inviscid predictions up to the mid-chord region where the viscous effects start to dominate towards the trailing edge exhibiting sensitivity of the laminar separation region to different flow conditions. The lift biases observed in Figs 9 and 11 with embedded (actuated or non-actuated) cavities for the airfoil in uniform flow correspond to the differences in mean pressure distributions on the suction and pressure sides. These biases are nearly removed in the non-uniform flow in Figs 13 and 14, with the mean pressure differences in Fig. 15 (top) limited to the regions downstream of the actuator's location.

The RMS surface pressures levels for both gust interaction cases in Fig. 15 (bottom) closely match with inviscid predictions up to the mid-chord region, with the pressure fluctuations enhanced towards the trailing edge due to the energized and gust phase-locked boundary-layer vorticity dynamics.

In general, the actuation cases clearly stand apart in Fig. 15 showing the mid-chord excitations both for the mean and RMS surface pressure on the suction side. Interestingly, downstream of the cavity the impact appears nearly identical for the gust and no-gust cases on the upper surface. In particular, the actuation time-periodic forcing of the boundary layer enhances the RMS surface pressure levels much above the non-actuated case with uniform upstream flow and even higher than the corresponding gust case. At the same time, the RMS pressure fluctuations are reduced at the trailing edge itself. In uniform flow, the actuation also appears to reduce RMS pressure levels on the upper surface upstream of the cavity and on the lower surface. On the other hand, in the gust case, the actuation effect is limited to the upper surface downstream of the cavity whereas the results are practically identical both for the mean and RMS surface pressure distributions upstream of the cavity and on the lower surface.

The acoustic directivities in Fig. 16 obtained at the radius r=1 from the airfoil mid-chord position show an adequate similarity with inviscid predictions [15] for the gust cases both in shape and magnitude. As shown in Ref. [12], the comparison

is much improved at high Reynolds numbers indicating an important contribution of the trailing-edge noise radiation in the current cases.

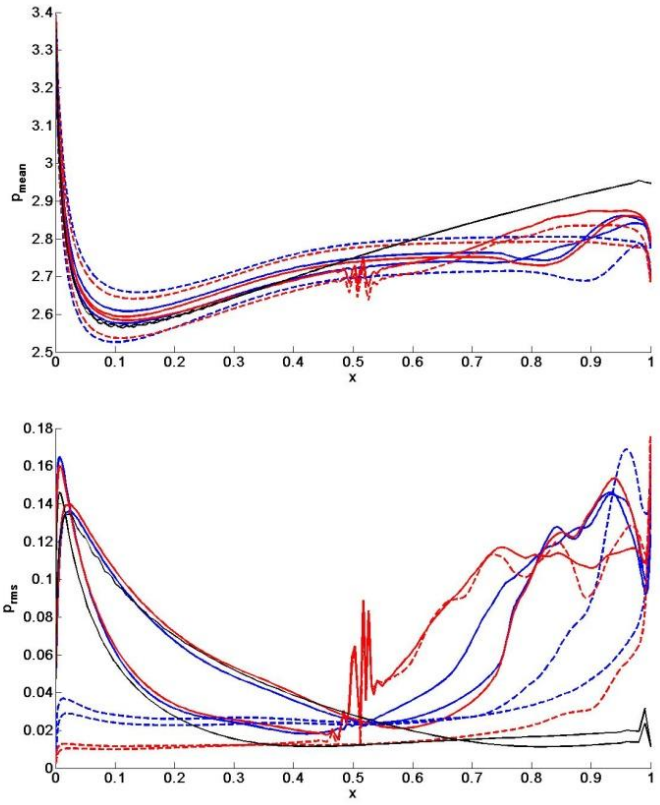

Figure 15. Mean (top) and RMS (bottom) airfoil surface pressure for cases with gust (solid lines) and without gust (dashed lines): without actuation (blue lines), with actuation (red lines); comparison with inviscid solutions (black lines).

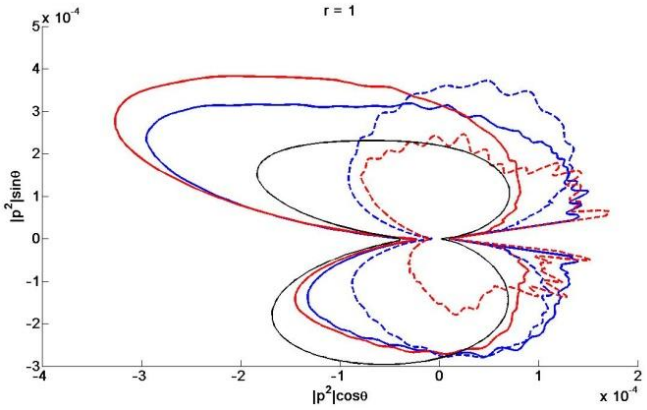

Figure 16. Scaled directivities of RMS acoustic intensity at r=1 for cases with gust (solid lines) and without gust (dashed lines): without actuation (blue lines), with actuation (red lines); comparison with inviscid solutions (black line).

As expected, the gust response case is barely affected by actuation showing a slight difference in the upper lobe orientation and amplitude possibly attributed to the enhanced RMS surface pressure downstream of the cavity. The effect of actuation on the trailing-edge noise (with uniform upstream flow), on the other hand, is more prominent showing acoustic intensity reduction in both directivity lobes attributed to the reduced RMS surface pressure levels at the trailing edge.

Future studies will further address the impact of the actuator location, frequency and excitation amplitude on the airfoil aerodynamics and acoustics.

CONCLUSIONS

A two-part high-fidelity numerical study investigated the effect of synthetic-jet actuation on airfoil flow and noise control. The actuator was modelled without its resonator cavity by imposing a fluctuating-velocity boundary condition at the bottom of the actuator's orifice, to allow the actuator's time-periodic jet to interact with the grazing flow. Only the actuator's orifice with properly defined boundary condition was thus embedded into the airfoil surface at a selected location. The ratio of the actuator's orifice width to the airfoil chord was fixed at d/c=0.005 in this study.

The first part considered SD7003 airfoil unsteady aerodynamic response in a laminar flow with M=0.1 and Re=10,000. The embedded actuator model was located about 0.3c downstream from the leading edge on the airfoil suction side in the area where a laminar separation zone formed in steady-state simulations. With the uniform upstream flow conditions, the airfoil lift response indicated a noticeable actuation effect. For the case of the incident large-amplitude sharp-edge gust, the stalled airfoil unsteady lift response was sensitive to actuation but the peak response values were primarily shifted and in some cases even increased indicating a limited SJA control authority for a massively separated flow. Importantly, the airfoil recovery back to the steady-state oscillations following the gust passage was expedited by actuation. The overall response appeared most subdued with actuation at shedding frequency.

The second part of the study considered both aerodynamic and acoustic responses of symmetric, 12%-thick, unloaded Joukowski airfoil in uniform and non-uniform transitional upstream flows at M=0.5 and Re=50,000. The actuator model was embedded at mid-chord on the suction side. The flow non-uniformity was modeled in terms of a time-harmonic gust, which allowed comparison with previously validated benchmark inviscid solutions. With uniform upstream flow, the cases with and without embedded cavity exhibited a periodic pattern associated with the unstable laminar separation region formed at the trailing edge and periodically switching its primary position between the airfoil suction and pressure sides. Such separation zones revealed amplified boundary-layer instabilities developing into large vortical structures scattered into acoustic waves at the trailing edge. Without the embedded cavity, the established self-sustained resonant feedback loop involving the growing instabilities and the upstream-propagating acoustic waves was suggested to be the primary mechanism of the tonal trailing-edge noise. The latter was

greatly reduced with embedded non-actuated cavity while the actuation produced further reduction in the trailing-edge noise due to redistribution of the spectral energy in the pressure signal. With the incident gust, the airfoil unsteady response was dominated by the time-periodic forcing of the boundary layer with the gust frequency. The latter induced a gust phase-locking mechanism triggering a time-periodic generation and shedding of large vortical structures on both sides of the airfoil in synch with the gust frequency. The gust-induced leading-edge noise remained practically unaffected by actuation for the selected SJA position. Future studies will examine the actuation effect on airfoil noise for various SJA locations, actuation frequencies and amplitudes.

ACKNOWLEDGEMENTS

The authors would like to acknowledge support for this work from the National Science Foundation, Award Number 0955970 (Program Manager Dr. H.H. Winter), and Florida Center for Advanced Aero Propulsion. The guidance obtained from Dr. Miguel Visbal (AFRL) and Dr. Scott Sherer (AFRL) in implementing high-accuracy numerical simulations is highly appreciated.

REFERENCES

[1] Ewert, R. and Manoha, E., (2007) "Trailing-Edge Noise," from "Large-Eddy Simulation for Acoustics," by Wagner, C., Huttle, T. and Sagaut, P., Cambridge University Press, pp. 293-333.

[2] Paterson, R., Vogt, P., Fink, M., and Munch, C., (1973), "Vortex Noise of Isolated Airfoils," J. Aircraft, Vol. 10, pp. 296-302.

[3] Arbey, H., and Bataille, J., (1983), "Noise Generated by Airfoil Profiles Placed in a Uniform Laminar Flow," J. Fluid Mechanics, Vol. 134, pp. 33-47

[4] Golubev, V.V., Nguyen, L., Roger, M., and Visbal, M.R., (2011), "On Interaction of Airfoil Leading and Trailing Edge Noise Sources in Turbulent Flow," *AIAA Paper* 2011-2859, 17th AIAA/CEAS Aeroacoustics Conference, Portland, June 2011.

[5] Visbal, M.R. and Gaitonde, D.V., (2002) "On the Use of High-Order Finite-Difference Schemes on Curvilinear and Deforming Meshes," Journal of Computational Physics, Vol. 181, pp.155–185.

[6] Golubev, V.V., Hollenshade, T.M., Nguyen, L., and Visbal, M.R., (2010), "Parametric Viscous Analysis of Gust Interaction with SD7003 Airfoil," AIAA Paper 2010-928.

[7] Golubev, V.V., Nguyen, L., and Visbal, M.R., (2010), "High-Accuracy Low-Re Simulations of Airfoil-Gust and Airfoil-Vortex Interactions," AIAA Paper 2010-4868.

[8] Golubev, V.V., Nguyen, L., and Visbal, M.R., (2011), "High-Fidelity Simulations of Transitional Airfoil Interacting with Upstream Vortical Structure," AIAA Paper 2011-394

[9] Rizzetta, D. P., Visbal, M.R., and Stanek, M.J., (1999), "Numerical Investigation of Synthetic-Jet Flowfields." AIAA J., Vol. 37, pp. 919-927.

[10] Suhs, N.E., Rogers, S.E., Dietz, W.E., (2002), "PEGASUS 5: An Automated Pre-processor for Overset-Grid CFD," AIAA Paper 2002-3186.

[11] Sherer, S.E., Visbal, M.R., Galbraith, M.C., (2006), "Automated Preprocessing Tools for Use with a High-Order Overset-Grid Algorithm," AIAA Paper 2006-1147.

[12] Raju, R., Aram, E., Mittal, R., Cattafesta, L., (2009), "Simple Models of Zero-Net Mass-Flux Jets for Flow Control Simulations," International Journal of Flow Control, Vol. 1, pp. 179-197.

[13] Scott, J.R., (2004), "Single Airfoil Gust Response Problem," Proceedings of the 4th CAA Workshop on Benchmark Problems, NASA CP-2004-212954, pp.45-48.

[14] Golubev, V.V., Nguyen, L., Visbal, M.R., (2010), "High-Fidelity Viscous Simulations of Airfoil Noise Radiation in Nonuniform Unsteady Flow," *AIAA* 2010-3761, 16th AIAA/CEAS Aeroacoustics Conference, Stockholm, Sweden, June 2010.

[15] Golubev, V.V., Mankbadi, R.R. and Hixon, R., (2004) "Simulation of Airfoil Response to Impinging Gust Using High-Order Prefactored Compact Code," Proceedings of the 4th CAA Workshop on Benchmark Problems, NASA/CP-2004-212954, Cleveland, OH, October 2003, pp. 141-148.